Bioactive Materials 6 (2021) 2841–2853

Contents lists available at ScienceDirect

Bioactive Materials

journal homepage: www.sciencedirect.com/journal/bioactive-materials

Development of a novel RNAi therapy: Engineered miR-31 exosomes promoted the healing of diabetic wounds

Jinghuan Huang [a,1], Muyu Yu [b,1], Wenjing Yin [a], Bo Liang [a], Ang Li [a], Jingfeng Li [c], Xiaolin Li [a,*], Shichang Zhao [a,**], Fang Liu [b,***]

[a] Department of Orthopaedic Surgery, Shanghai Jiao Tong University Affiliated Sixth People's Hospital, China
[b] Department of Endocrinology and Metabolism, Shanghai Jiao Tong University Affiliated Sixth People's Hospital, China
[c] Department of Orthopedics, Zhongnan Hospital of Wuhan University, China

ARTICLE INFO

Keywords:
Engineered exosomes
Diabetes chronic wounds
RNAi therapy
miR-31-5p
Precision therapy

ABSTRACT

Rationale: Chronic wounds associated with diabetes exact a heavy burden on individuals and society and do not have a specific treatment. Exosome therapy is an extension of stem cell therapy, and RNA interference (RNAi)-based therapy is a type of advanced precision therapy. Based on the discovery of chronic wound-related genes in diabetes, we combined exosome therapy and RNAi therapy through an engineering approach for the treatment of diabetic chronic wounds. Methods: We combined exosome therapy and RNAi therapy to establish a precision therapy for diabetes-associated wounds via an engineered exosome approach. Results: First, chronic diabetic wounds express low levels of miR-31-5p compared with nondiabetic wounds, and an miR-31-5p mimic was shown to be effective in promoting the proliferation and migration of three wound-related cell types in vitro. Second, bioinformatics analysis, luciferase reporter assays and western blotting suggested that miR-31-5p promoted angiogenesis, fibrogenesis and reepithelization by inhibiting factor-inhibiting HIF-1 (HIF1AN, also named FIH) and epithelial membrane protein-1 (EMP-1). Third, engineered miR-31 exosomes were generated as a miR-31-5p RNAi therapeutic agent. In vivo, the engineered miR-31 exosomes promoted diabetic wound healing by enhancing angiogenesis, fibrogenesis and reepithelization. Conclusion: Engineered miR-31 exosomes are an ideal disease pathophysiology-initiated RNAi therapeutic agent for diabetic wounds.

1. Introduction

Chronic wounds, which have delayed closure due to various pathological factors, cause economic and social burdens as well as psychological trauma. As aging populations increase, chronic wounds are increasing dramatically due to many age-related diseases, such as diabetes mellitus. Diabetic wound healing is often delayed and results in substantial morbidity, impaired quality of life, and even lower extremity amputation. Under high glucose conditions, endothelial cells, epidermal cells, fibroblasts and inflammatory cells are dysfunctional, which delays the wound-healing process [1–4]. Currently, diabetic chronic wounds remain a difficult problem for orthopedic surgeons and endocrinologists [5]. Traditional therapies for diabetic chronic wounds are conservative and include optimized glycemic control, dressing changes, debridement and antibiotic administration as the major treatment choices for chronic diabetic wounds. However, these approaches focus on creating a more favorable environment for wound healing or on halting disease progression, such as amputation. These measures do not result in satisfactory outcomes in every case, but a curative and more aggressive therapy is still lacking because the pathophysiology is largely unknown. To achieve a curative and more aggressive therapy, we focused on precision therapy.

Precision therapy, which emphasizes specific treatment according to the disease pathophysiology, has provided renewed hope for many diseases, including diabetic chronic wounds. MicroRNAs (miRNAs) play a significant role in disease pathophysiology. On the one hand, miRNAs

Peer review under responsibility of KeAi Communications Co., Ltd.
* Corresponding author. Shanghai Jiao Tong University Affiliated Sixth People's Hospital, Yishan Road 600, Shanghai, 200233, China.
** Corresponding author. Shanghai Jiao Tong University Affiliated Sixth People's Hospital, Yishan Road 600, Shanghai, 200233, China.
*** Corresponding author. Shanghai Jiao Tong University Affiliated Sixth People's Hospital, Yishan Road 600, Shanghai, 200233, China.
E-mail addresses: lixiaolin@sjtu.edu.cn (X. Li), zhaoshichang0404@163.com (S. Zhao), f-liu@sjtu.edu.cn (F. Liu).
[1] Jinghuan Huang and Muyu Yu contributed equally to this work.

https://doi.org/10.1016/j.bioactmat.2021.02.007
Received 22 December 2020; Received in revised form 23 January 2021; Accepted 9 February 2021

regulate complex physiological and pathophysiological processes by targeting multiple genes. On the other hand, miRNAs can be potential therapeutic molecules by supplementing pathologically reduced miRNAs and targeting specific disease-causing genes [6,7]. Therefore, miRNA-interference-based (miRNAi) therapy, a type of RNAi therapy, can be an important approach in precision therapy [8]. However, one of the two key aspects of miRNAi therapy is the identification of pathologically reduced miRNAs and specific disease-causing genes.

The other key aspect of miRNAi therapy is the carrier [9]. Immunological reactions, instability in the extracellular environment, low bioavailability and an inability to cross certain barriers are drawbacks of miRNAs in therapeutic applications [10,11]. Nanomaterials, which can protect and deliver miRNAs, have become crucial in miRNAi therapy implementation [12,13]. However, due to the potential biotoxicity of many organic and inorganic nanomaterials, the clinical use of artificial nanomaterials to implement miRNAi therapy is limited. Recently, a biogenetic derivative nanosized vesicle has attracted the attention of many scholars and has been well developed. Exosomes, which are extracellular vesicles (EVs) 30–150 nm in diameter, contain proteins, RNAs, and DNAs, among other molecules [14]; they are regarded as a tool for cell-cell communication and are optimal nanodelivery carriers due to their capacity to carry large cargos and to protect their contents from enzymes and chemicals [15–17]. Compared with artificial nanomaterials, exosomes have minor immunogenicity and biotoxicity, and therefore, they have greater biosafety properties [18].

In this study, we developed a precise therapeutic agent based on diabetic wound pathophysiology. Using patient samples and in vitro studies, we discovered that miR-31-5p plays an important role in diabetic wound pathophysiology. The involvement of the HIF pathway and the EMP-1-associated mechanism of miR-31-5p in regulating three wound-related cell lines were also revealed. Based on our findings, we constructed and produced engineered exosomes (engineered miR-31 exosomes), as an agent based on precision therapy to treat this disease. In vitro and in vivo assessments were performed, and the results show that the engineered miR-31 exosomes promoted diabetic wound healing via angiogenesis, fibrogenesis and reepithelization. The engineered miR-31 exosomes, a disease-driven biogenetic therapeutic agent, achieved precision treatment of diabetic wounds.

2. Materials and methods

This study was performed under the approval of the Ethics Committee of Shanghai Sixth People's Hospital, Shanghai Jiao Tong University School of Medicine, and complied with the principles of the Declaration of Helsinki. Written informed consent was provided by each donor with permission of the Institutional Review Board of Shanghai Sixth People's Hospital (Approval no.: 2018-022, Date of review: 2018-03-29). All animal experiments were approved by the Animal Research Ethics Committee of Shanghai Sixth People's Hospital and conducted according to the National Institutes of Health Guidelines for the Care and Use of Laboratory Animals.

2.1. Wound tissue collection and miR-31-5p detection

Nondiabetic wound tissues were obtained from the wound edges of patients who underwent second-stage (day 7) amputation (patients who selected a second-stage amputation to save other limbs after undergoing severe limb trauma) (n = 6). Chronic diabetic wound tissues were obtained from the wound edges of patients who underwent a diabetic foot amputation (n = 6). When debridement was performed, the necrotic tissue was removed until skin tissue with an adequate blood supply was reached. We trimmed the edge of the skin tissue with an adequate blood supply for quantitative real-time polymerase chain reaction (qRT-PCR) and *in situ* hybridization. All patients were treated at the Orthopedic Department of Shanghai Sixth People's Hospital, Shanghai, China. MiR-31-5p levels in the samples were detected by qRT-PCR and *in situ* hybridization. For *in situ* hybridization, briefly, xylene, ethanol and diluted DPEC (Amresco, USA) were used to deparaffinize the sections. After deparaffinization, the sections were boiled in antigen retrieval solution and digested in proteinase K (20 μg/ml) working solution (Servicebio, China). The sections were prehybridized using prehybridization solution (Servicebio) and then hybridized with probe hybridization solution (Servicebio, miR-31-5p probe: 5′-AGCTATGCCAGCATCTTGCCT-3′) overnight. After washing and blocking with rabbit serum, the sections were incubated with alkaline phosphatase-conjugated IgG fraction monoclonal mouse anti-digoxin antibody (anti-DIG-AP, Jackson, India) after which staining was visualized with the NBT/BCIP chromogenic reagent (Boster, USA).

2.2. In vitro cell responses to miR-31-5p

Human keratinocytes (HaCaTs) were kindly provided by Dr. Yiwen Yang, Dermatology Department, Huashan Hospital, Shanghai, China. Human fibroblasts (HFF-1), EA.hy926 cells (endothelial cells, ECs) and human embryonic kidney 293 cells (HEK293) were obtained from American Type Culture Collection (ATCC) and the Cell Bank of the Chinese Academy of Sciences, respectively. HaCaTs, ECs and HEK293 cells were cultured in Dulbecco's Modified Eagle's Medium (DMEM, Gibco, Invitrogen, Australia) supplemented with 10% fetal bovine serum (FBS, Gibco, Invitrogen), 100 U/ml penicillin and 100 μg/ml streptomycin (Invitrogen) at 37 °C. For ECs, a 1% endothelial cell growth supplement/heparin kit (ECGS/H, Promocell, Germany) was also used. HFF-1 cells were cultured in high-glucose DMEM supplemented with 15% FBS, 100 U/ml penicillin and 100 μg/ml streptomycin at 37 °C.

The proliferation of HaCaT, ECs and HFF-1 cells under different conditions was evaluated using a cell viability assay [Cell Counting Kit-8 (CCK-8), Dojindo Molecular Technologies, Japan]. Briefly, 2000 HaCaTs, ECs and HFF-1 cells per well were treated with different factors [PBS (control), mimic-nc (50 nM, RiboBio, China), miR-31-5p mimic (50 nM, RiboBio) and/or si-HIF1A (50 nM, RiboBio)] in 96-well plates. On days 1, 3 and 7, the culture medium was replaced with 10% culture medium containing CCK-8 solution. After incubation for 1 h at 37 °C, the absorbance of each well was measured at 450 nm using a spectrophotometric microplate reader (Bio-Rad 680, USA).

Cell migration was observed using a Transwell assay. For mimic interference, cells were pretreated with PBS (control), mimic-nc (50 nM), miR-31-5p mimic (50 nM) and/or si-HIF1A (50 nM) for 2 days (for exosome interference, the cells were not pretreated). Briefly, 20,000 HaCaTs, ECs or HFF-1 cells were seeded into the upper chamber of a Transwell plate (Corning, USA); culture medium was added to the lower chamber. After 24 h (48 h for HFF-1 cells), the cells on the upper surface of the membrane were removed using cotton swabs. The cells on the lower surface were fixed and stained with 0.5% crystal violet. Then, the results were observed via optical microscopy.

To assess the effect of the miR-31-5p mimic on EC capillary-like construction activity, tube formation in ECM gel (Sigma-Aldrich, Germany) was observed. Briefly, cold ECM gel was transferred into a 24-well plate at 200 μl/well. For mimics, ECs were pretreated with PBS (control), mimics (mimic-nc, miR-31-5p mimic, 50 nM) or si-HIF1A (50 nM) for 2 days (for exosome interference, the cells were not pretreated). Then, a 200-μl suspension of pretreated ECs (80,000 cells) was overlaid on the ECM gel. Eight hours later, tube formation was observed via light microscopy.

Vascular endothelial growth factor (VEGF) and type I collagen (COL I) are crucial factors in angiogenesis and fibrogenesis. To investigate the effect of miR-31-5p on the expression of VEGF/COL1 in ECs/HFF-1 cells, VEGF/COL I immunofluorescence assays and enzyme-linked immunosorbent assays (ELISAs) were performed. For immunofluorescence, 10,000 ECs or HFF-1 cells were seeded into a 24-well plate and incubated with PBS (control, 10 μl), mimic-nc (50 nM) or miR-31-5p mimic (50 nM) for 48 h. The cells were then fixed in 2.5% glutaraldehyde for 20 min. An anti-VEGF antibody (ABclonal, USA) or anti-COL I antibody

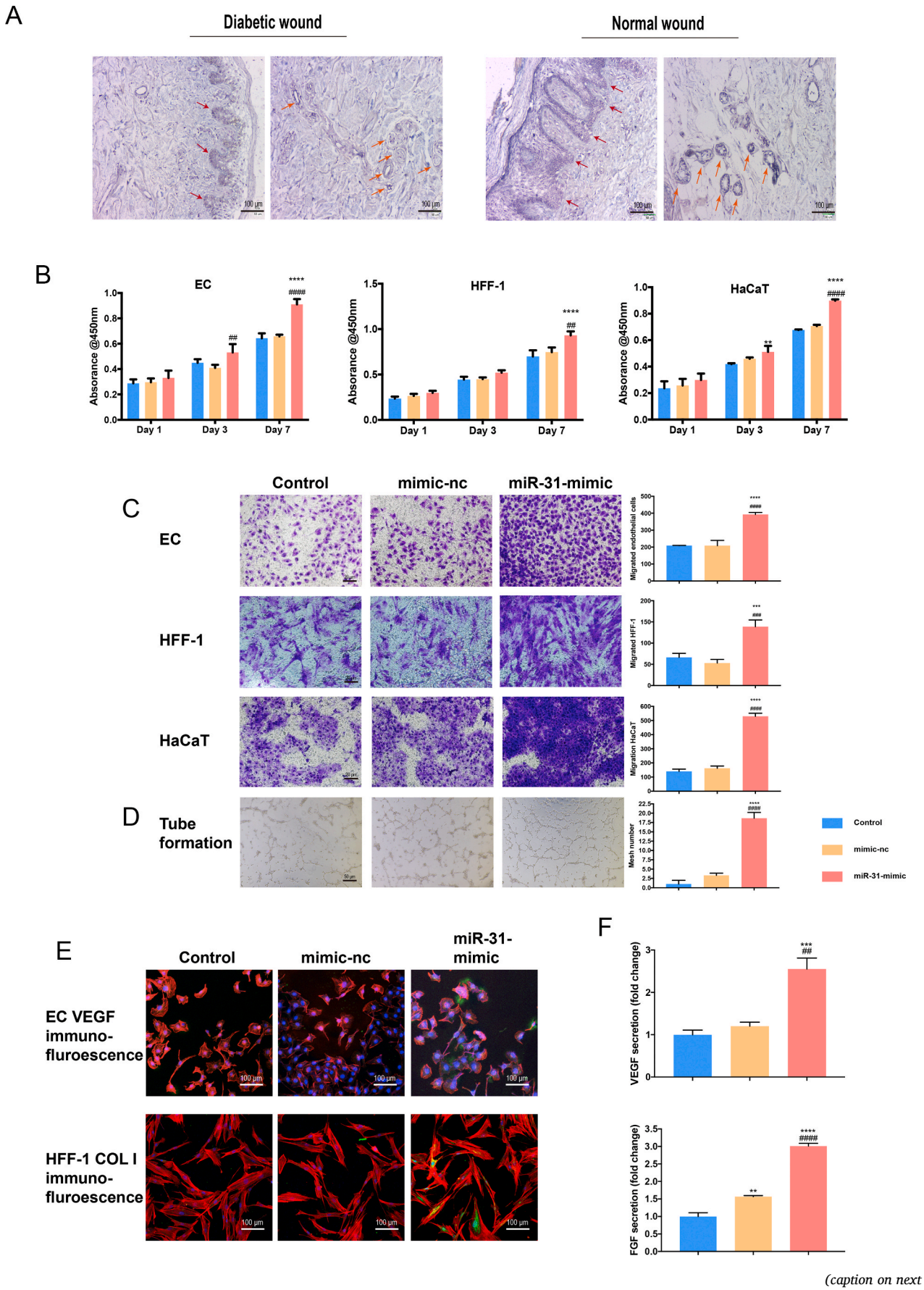

(caption on next page)

Fig. 1. MiR-31-5p expression is reduced in diabetic wounds and is important in wound healing. (A) *In situ* hybridization of miR-31-5p in diabetic and normal wounds; (B) miR-31-5p effects on ECs, HFF-1 cells and HaCaT cell proliferation; (C) miR-31-5p effects on ECs, HFF-1 cells and HaCaT cell migration; (D) miR-31-5p effects on EC capillary-like structure formation; (E) VEGF/COL I immunofluorescence in EC/HFF-1 cells under miR-31-5p interference (red represents the cell cytoskeleton; green represents VEGF or COL I; blue represents nuclei); (F) VEGF/COL I ELISA of EC/HFF-1 cells under miR-31-5p interference; *significant difference compared with control ($p < 0.05$); **significant difference compared with control ($p < 0.01$); ***significant difference compared with control ($p < 0.001$); ****significant difference compared with control ($p < 0.0001$); # significant difference compared with mimic-nc ($p < 0.05$); ## significant difference compared with mimic-nc ($p < 0.01$); ### significant difference compared with mimic-nc ($p < 0.001$); #### significant difference compared with mimic-nc ($p < 0.0001$).

(ABclonal) was added to each well and incubated with the cells at 37 °C overnight. A secondary antibody was added after the primary antibody was removed and incubated with the cells at 37 °C for 1 h. Next, to visualize the nuclei, the samples were stained with DAPI for 5 min (blue, Sigma-Aldrich, Germany), and to visualize the cytoskeleton, the samples were stained with phalloidin for 40 min (red, Thermo Fisher) after which they were observed using a confocal laser scanning microscopy. For ELISA, 100,000 ECs or HFF-1 cells were seeded in 6-well plates and treated with PBS (control, 10 μl), mimic-nc (50 nM) or miR-31-5p mimic (50 nM) for 3 days. Then, the supernatants were collected, and VEGF and FGF were detected using an ELISA kit (NeoBioscience, China) in accordance with the manufacturer's instructions.

2.3. Mechanism of action of miR-31-5p

MiR-31-5p targets were predicted using TargetScan, StarBase and miRDB. The three sets of results were overlaid, and the common target genes were considered highly confident targets. To identify proangiogenesis, profibrogenesis and reepithelization targets of miR-31-5p, anti-angiogenesis, anti-fibrogenesis and anti-epithelization gene pools were constructed by Gene Otology and article review. Highly confident targets of miR-31-5p were overlaid with the anti-angiogenesis, anti-fibrogenesis and anti-epithelization gene pools, and the possible targets were identified.

The HIF1AN and EMP-1 3′-UTRs containing luciferase reporter plasmids and empty luciferase vectors were purchased (Obio, China), and the mutation sites were predicted binding sites of miR-31-5p that were fabricated. Mutations were verified by sequencing. Cells were cotransfected with plasmids at 200 ng/ml and pre-miR-control or pre-miR-31-5p using Lipofectamine 2000 (Invitrogen). Forty-eight hours later, luciferase activity was estimated using a Dual-Luciferase Reporter Assay System (Promega, China) according to the manufacturer's instructions.

A microRNA Reverse Transcription kit (EZbioscience, USA) and microRNA qPCR kit (EZbioscience) were used for qRT-PCR to detect miRNA content. qRT-PCR was performed according to the manufacturer's instructions. The results were normalized to those of RNU6B The primers used are listed below: miR-31-5p reverse transcription primer sequence: 5'– GTCGTATCCAGTGCAGGGTCCGAGGTATTCGCACTGGATACGACAGCTAT –3'; PCR primer sequence: forward: 5'– GCGAGGCAAGATGCTGGC –3'; reverse: 5'– AGTGCAGGGTCCGAGGTATT –3′) and RNU6B (RNU6-1 reverse transcription primer sequence: 5'– GTCGTATCCAGTGCAGGGTCCGAGGTATTCGCACTGGATACGACAAA ATA–3'; PCR primer sequence: forward: 5'– AGAGAAGATTAGCAT GGCCCCTG –3'; reverse: 5'– ATCCAGTGCAGGGTCCGAGG –3′). Western blotting was performed according to previous reports [19]. HaCaT, ECs and HFF-1 cells were pretreated with PBS (control), mimic-nc (50 nM), miR-31-5p mimic (50 nM), si-HIF1A (50 nM) or si-nc (50 nM, RiboBio) for 2 days. Then, the total proteins of cells were extracted for western blot analysis. Anti-Tsg101, anti-CD9 antibodies were purchased from abcam; anti-Alix, anti-Calnexin, anti-HIF1AN and anti-VEGF antibodies were purchased from Proteintech, USA, and the anti-EMP-1 antibody was purchased from Absin, Shanghai.

2.4. Engineered miR-31-5p exosome preparation and identification

A miR-31-5p lentiviral vector was purchased from GenePharma, Shanghai. According to the manufacturer's instructions, HEK293 cells were incubated with retroviral supernatant and 5 μg/ml polybrene for 24 h. Infected HEK293 cells were selected by puromycin dihydrochloride (Thermo Fisher).

When HEK293 and transfected HEK293 cells reached 50% confluence, the supernatants were replaced with MesenGro hMSC medium (StemRD, USA), and the cells were cultured for 48 h. Then, the conditioned medium (CM) was harvested to isolate exosomes. Briefly, the CM was centrifuged at 300×*g* (15 min) and 2000×*g* (15 min) to remove dead cells and debris. To further remove cellular debris, a 0.22-μm filter (Merck Millipore, USA) was used. Then, the solution was ultracentrifuged at 100,000×*g* (90 min) in an ultracentrifuge (Beckman, USA). The supernatant was removed, and the pellets were resuspended in PBS and ultracentrifuged again at 100,000×*g* (90 min). The pellets were then resuspended in PBS. All parts of this procedure were performed at 4 °C. Nanoparticle Tracking Analysis was used to quantify exosomes.

Transmission electron microscopy (TEM) was used to observe exosome morphology. Dynamic light scattering (DLS) was applied to measure the size distribution of the exosomes. Exosomal characteristic markers (CD9, Alix, Tsg101 and Calnexin) were detected by western blotting. qRT-PCR was performed to evaluate miR-31-5p content in the exosomes.

2.5. In vitro response of cells to the engineered miR-31 exosomes

To observe the effects of engineered miR-31 exosomes on three wound-related cell lines (ECs, HFF-1 cells, HaCaTs), exosome uptake was first determined. Exosomes were stained with PKH26 (Sigma-Aldrich) according to the manufacturer's instructions. Fluorescence-labeled exosomes were cocultured with the three wound cell lines in 24-well plates for 24 h. Then, the cells were stained with phalloidin (45 min) and DAPI (5 min). Exosome uptake was observed by laser confocal microscopy. To assess whether miR-31-5p was successfully transfected into cells via exosomes, cellular miR-31-5p content was detected via qRT-PCR. Cell proliferation (CCK-8 assay), migration (Transwell assay), and tube formation assays were performed with cells as previously described. For the CCK-8 assay, cells were treated with PBS (control), nonengineered HEK293 exosomes (1×10^9) or engineered miR-31 exosomes (1×10^9) for 1, 3 or 7 days. To evaluate cell migration, PBS (control), nonengineered HEK293 exosomes (1×10^9) or engineered miR-31 exosomes (1×10^9) were added to the culture medium in the lower chamber. To evaluate EC tube formation, PBS (control), nonengineered HEK293 exosomes (1×10^9) or engineered miR-31 exosomes (1×10^9) were added to the suspension of ECs on the ECM gel.

2.6. In vivo studies of engineered miR-31 exosomes in chronic diabetic wound closure

Thirty-six male Sprague-Dawley (SD) rats (12 weeks old, 250–300 g) were used in this study. Streptozotocin (STZ; Sigma-Aldrich) was used to induce diabetes. STZ was dissolved in 0.1 M phosphate-citrate buffer and injected intraperitoneally into SD rats at a dose of 55 mg/kg. Blood samples were collected from SD rat tail veins and measured using a glucometer (Roche, Switzerland). Skin wounds were generated once the blood glucose levels were >250 mg/ml, which indicated diabetes. After anesthesia with an intraperitoneal injection of 1 ml/kg of 3% pentobarbital sodium (Sigma-Aldrich), the dorsal fur was shaved with a razor. Defect areas were marked with a pen, and standardized full-thickness

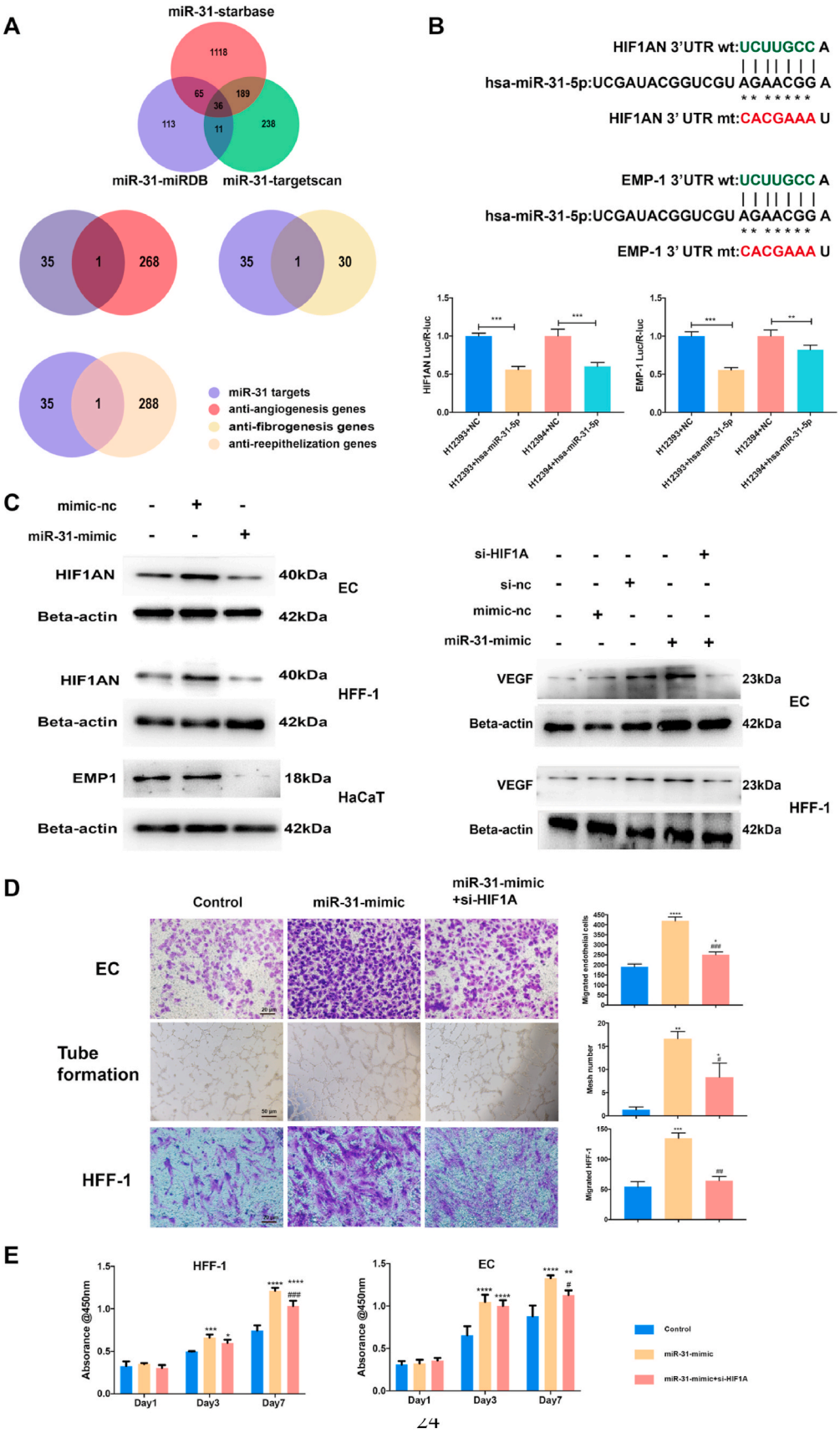

Fig. 2. MiR-31-5p regulates endothelial cells, fibroblasts and epithelial cells via the HIF pathway and EMP-1. (A) miR-31-5p target prediction according to StarBase, miRDB and TargetScan; miR-31-5p endothelial cells, fibroblasts and epithelial cells regulating targets found by intersections of possible miR-31-5p targets and the anti-angiogenesis gene pool, anti-fibroblast gene pool or anti-reepithelization gene pool; (B) miR-31-5p inhibition of HIF1AN and EMP-1 as detected by luciferase assays; (C) western blotting shows HIF1AN, VEGF and EMP-1 expression in ECs, HFF-1 cells and HaCaT cells with miR-31-5p-mimic and si-HIF1A treatment; (D) EC and HFF-1 cell migration and EC tube formation under treatment with miR-31-5p-mimic and si-HIF1A; (E) EC and HFF-1 cell proliferation under treatment with miR-31-5p-mimic and si-HIF1A. *Significant difference compared with control ($p < 0.05$); **significant difference compared with control ($p < 0.01$); ***significant difference compared with control ($p < 0.001$); ****significant difference compared with control ($p < 0.0001$); # significant difference compared with miR-31-5p mimic ($p < 0.05$); ## significant difference compared with miR-31-5p mimic ($p < 0.01$); ### significant difference compared with miR-31-5p mimic ($p < 0.001$); #### significant difference compared with miR-31-5p mimic ($p < 0.0001$).

skin wounds were generated (diameter = 2.0 cm). The rats were then randomly assigned into 4 different groups, which were treated with PBS (control), nonengineered HEK293 exosomes (1×10^{11}), engineered miR-31 exosomes (5×10^{10}) or engineered miR-31 exosomes (1×10^{11}). PBS or exosomes were injected around the wound at 4 injection sites and applied to the wound bed. Then, gauze was used to cover the wounds. At days 0, 3, 7 and 14 after the procedure, the gauze covers were removed, and the wounds were observed. Wound closure was calculated according to the following equation: wound closure (%) = (AO - At)/AO × 100, where AO is the initial wound area, and At is the wound area on the observation days.

The rats were sacrificed on days 7 and 14 after the procedure, and the wound tissues containing the wound bed and surrounding healthy skin were carefully collected. The wound tissue samples were fixed in formalin, subjected to dehydration in graded alcohol solutions and embedded in paraffin. Sections (~5 μm) were generated and stained with H&E and Masson's trichrome. The neoepithelium length was measured under a light microscopy.

Immunofluorescence was applied to assess CD31, a marker of ECs (1:50, Abcam, USA), and alpha-smooth muscle actin (α-SMA), a marker of vascular smooth muscle cells (1:200, Abcam). Both CD31 and α-SMA were used to estimate angiogenesis. The sections were rehydrated, blocked with 1.5% goat serum (Merck Millipore) and incubated with a primary antibody at 4 °C overnight. Alexa Fluor 488 and Cy3-conjugated secondary antibodies (Servicebio) were used, and DAPI was used to stain the nuclei. Samples were observed by confocal laser microscope. Immunohistochemistry was used to assess CD31 expression (1:100, Abcam). After rehydration, the sections were incubated with primary antibodies at 4 °C overnight. To visualize, a biotinylated secondary antibody and avidin-biotin-peroxidase complex (Servicebio) were used along with DAB substrate (DAKO, USA). Next, the sections were counterstained in hematoxylin and analyzed by light microscopy.

To assess blood vessel regeneration, Microfil (Microfil MV-122; Flow Tech, Carve) was used to perfuse the rats. Briefly, after anesthetization, the chest of each rat was opened using scissors. After ligating the bilateral pulmonary trunks, the inferior vena cava was punctured. Heparinized saline (100 ml) was perfused into the left ventricle through an angiocatheter, and 20 ml of Microfil was perfused at a rate of 2 ml/min into the left ventricle, then the ascending aorta was ligated. The samples were maintained at 4 °C overnight to ensure polymerization. The samples were then scanned using micro-CT (Skyscan 1176, Belgium) at a resolution of 9 μm and were reconstructed using 3D Creator software. The blood vessel area and number were determined using software.

2.7. Statistical analysis

All experiments were performed in triplicate unless otherwise specified. The results are expressed as the mean ± SD. Student-Newman-Keuls post hoc tests and ANOVA tests were used to conduct statistical analyses, and a p value < 0.05 was considered significant.

3. Results and discussion

3.1. MiR-31-5p is expressed at low levels in diabetic chronic wounds and plays an important role in wound healing

In patient wound samples, miR-31-5p was expressed at low levels in both the dermal and corium layers. MiR-31-5p expression in normal wounds and diabetic chronic wounds was assessed by *in situ* hybridization and qRT-PCR, and the results are shown in Figs. 1A and S1. According to *in situ* hybridization, miR-31-5p was expressed in both the epidermal and corium layers and in epithelial cells, fibrocytes and endothelial cells. Diabetic chronic wounds exhibited lower miR-31-5p expression than normal wounds in both skin layers and in the three cell types examined. qRT-PCR results further confirmed the *in situ* hybridization results. Therefore, we hypothesize that miR-31-5p may play a role in wound healing in the three cell types. Further evidence was obtained in an in vitro study. The results showed that the miR-31-5p mimic promoted the proliferation (Fig. 1B) and migration (Fig. 1C) of the three cell types. EC tube formation (Fig. 1D) was also enhanced by the miR-31-5p mimic. Two crucial factors in angiogenesis and fibrogenesis, VEGF and COL I (Fig. 1E), were observed by immunofluorescence and ELISA (Fig. 1F); the results showed that the miR-31-5p mimic positively regulated the angiogenic and fibrogenic abilities of ECs and HFF-1 cells. Fig. 1 shows that miR-31-5p is important in wound healing, yet diabetic chronic wounds expressed low levels of miR-31-5p. Therefore, miR-31-5p may be a crucial factor in diabetic chronic wounds, and miR-31-5p may be a multifunctional factor in precision therapy for diabetic chronic wounds.

3.2. MiR-31-5p functions in three wound cell types via the HIF pathway and EMP-1

MiR-31-5p is considered important in diabetic chronic wound etiology; however, the exact mechanism is still unclear. Therefore, we used bioinformatics to identify targets and related pathways. Three major miRNA target databases were searched to identify possible targets. According to the intersecting results, we reduced the scope of investigation and obtained 36 probable targets (Fig. 2A). Based on the intersection of 36 targets and the anti-angiogenesis, anti-fibrogenesis and anti-epithelization gene pools (Fig. 2A), we obtained one common target for angiogenesis and fibrogenesis, HIF1AN, and one target for epithelization, EMP-1. Luciferase reporter assays were used to evaluate the effects of miR-31-5p inhibition on HIF1AN and EMP-1 (Fig. 2B). Both HIF1AN and EMP-1 were inhibited by miR-31-5p; however, the HIF1AN luciferase reporter results did not show a rescue effect when site mutations were present, which indicates that there may be multiple miR-31-5p target sites in HIF1AN. Western blot results confirmed the luciferase reporter results (Fig. 2C).

HIF1AN is a major inhibitor of HIF-1α and is therefore a key inhibitor of the HIF pathway [21], which plays a crucial role in angiogenesis and fibrogenesis [22,23]; therefore, using western blotting, we evaluated the HIF pathway downstream of the key molecule VEGF (Fig. 2C). The results showed that miR-31-5p promoted VEGF expression and that this promotion could be rescued via HIF-1α inhibition. EC and HFF-1 cell proliferation, migration, and tube formation assay results also confirmed that miR-31-5p regulated angiogenesis and fibrogenesis via the HIF pathway (Fig. 2D and E). EMP-1 encodes the emp-1 protein, an intercellular adhesion molecule in keratinocytes that inhibits keratinocyte proliferation and migration [24]. MiR-31-5p inhibited emp-1 expression, and HaCaT cell proliferation and migration were also promoted by miR-31-5p, which indicates that miR-31-5p has a regulatory role in angiogenesis, fibrogenesis and epithelization.

Moreover, some scholars have found that the HIF pathway plays a role in the physiology and pathology of keratinocytes [25–27]. Therefore, we conducted supplemental experiments to determine whether miR-31-5p regulates reepithelization not only through EMP-1 but also through the HIF pathway. First, western blotting revealed that miR-31-5p inhibits HIF1AN expression in HaCaT cells (Fig. S3). Second, the promoting effect of miR-31-5p on HaCaT cell migration was rescued through si-HIF1A interference (Fig. S4), which indicates that the HIF pathway is also a regulatory way of miR-31-5p in reepithelization.

3.3. Engineered miR-31 exosomes effectively stimulate three wound-related cell types in vitro

As a key factor in diabetic wound pathophysiology and a multifunctional factor in angiogenesis, fibrogenesis and epithelization, miR-31-5p could be a potential precision therapy for diabetic wounds. MiRNA can transform from a physiological molecule to a therapeutic molecule. Some miRNA derivatives can be used clinically as drugs

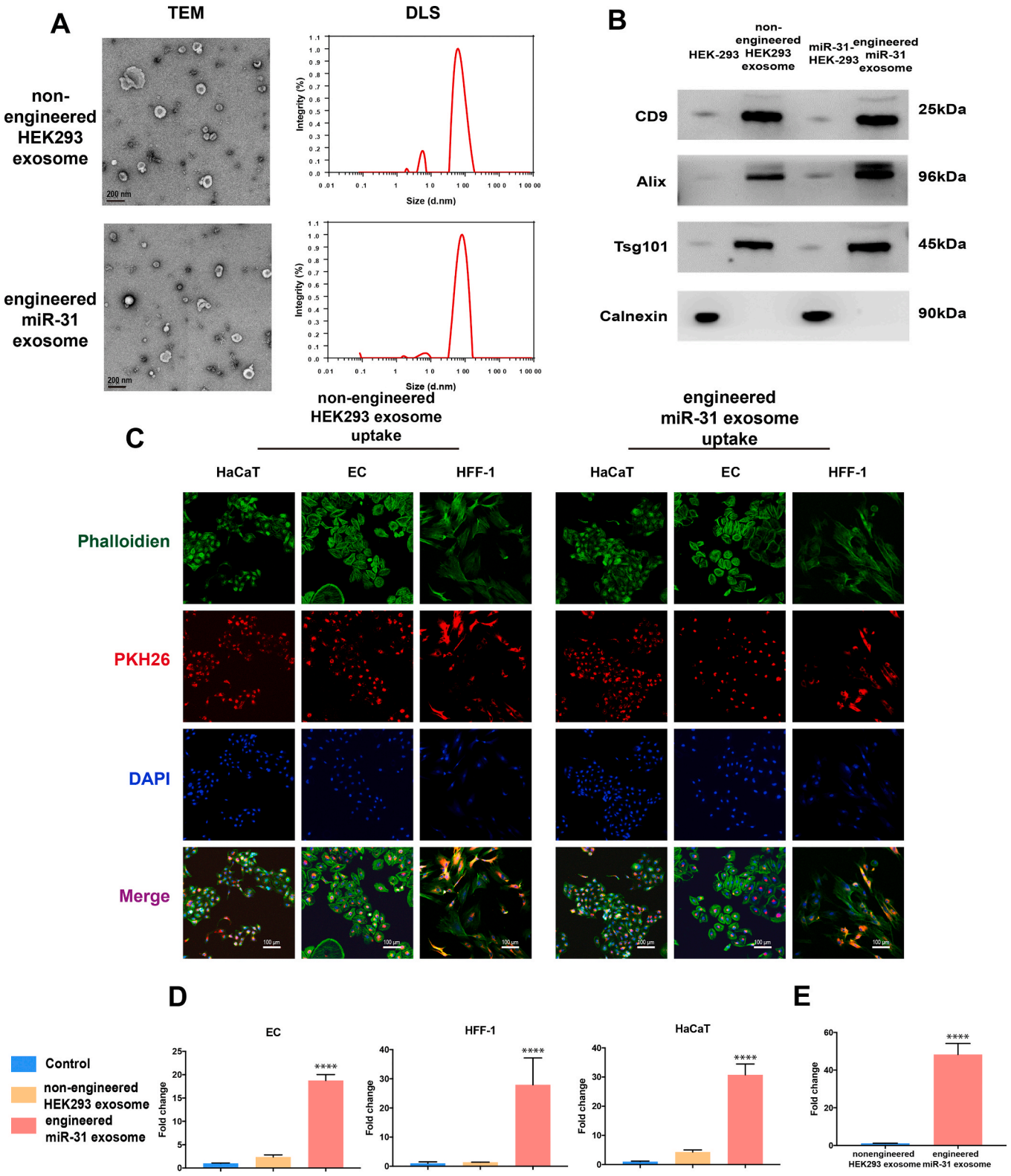

Fig. 3. Engineered miR-31 exosome insolation and characterization. (A) Nonengineered HEK293 exosome and engineered miR-31 exosome morphology and diameter distribution, as detected by TEM and DLS; (B) exosome surface markers detected by western blotting; (C) exosome internalization by ECs, HFF-1 cells and HaCaT cells; (D) miR-31-5p content in ECs, HFF-1 cells and HaCaT cells under different exosome conditions, ***significant difference compared with control ($p < 0.0001$); (E) miR-31-5p content in exosomes.

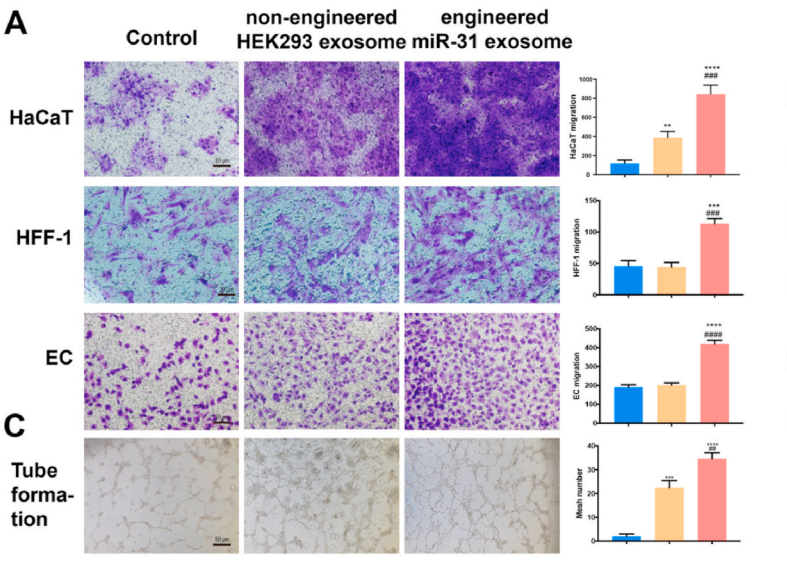

Fig. 4. Multiple functions of engineered miR-31 exosomes. (A) migration of ECs, HFF-1 cells and HaCaT cells; (B) proliferation of ECs, HFF-1 cells and HaCaT cells; (C) EC tube formation; *significant difference compared with control ($p < 0.05$); **significant difference compared with control ($p < 0.01$); ***significant difference compared with control ($p < 0.001$); ****significant difference compared with control ($p < 0.0001$); # significant difference compared with nonengineered HEK293 exosomes ($p < 0.05$); ## significant difference compared with nonengineered HEK293 exosomes ($p < 0.01$); ### significant difference compared with nonengineered HEK293 exosomes ($p < 0.001$); #### significant difference compared with nonengineered HEK293 exosomes ($p < 0.0001$).

[28–30]; however, a barrier-restricted RNAi therapy is the carrier [6,31,32]. For miRNAi therapy in this study, we selected exosomes as the carrier. Exosomes are cell-secreted vesicles 30-150-nm in diameter that are considered important intercellular communication tools. However, exosomes are also biogenetic therapeutic agents. Exosomes have some natural advantages, one of which is a lack of cytotoxicity [18]. Many nanomaterials cannot be applied in the clinic due to uncertain biotoxicity and metabolic processes, but exosomes have a high biosafety profile [33]. Exosomes can be obtained from patient autologous cells, and since they would have the same genetic background as the patient, exosomes are a personalized and precise therapy. Some studies have reported that exosomes themselves exert repair effects on tissues, including wounds [34–37]. High flexibility is another advantage, as exosomes can be engineered or modulated in the lipid layer and customized for surface molecules and content [38–40]. In this study, we engineered the exosome content by adding miR-31-5p via construction of an miR-31-5p-overexpressing cell line. Modified cells therefore became engineered miR-31-5p exosome factories that assembled miR-31-5p into exosomes to produce the therapeutic agent.

Cell lines overexpressing miR-31-5p were constructed by viral

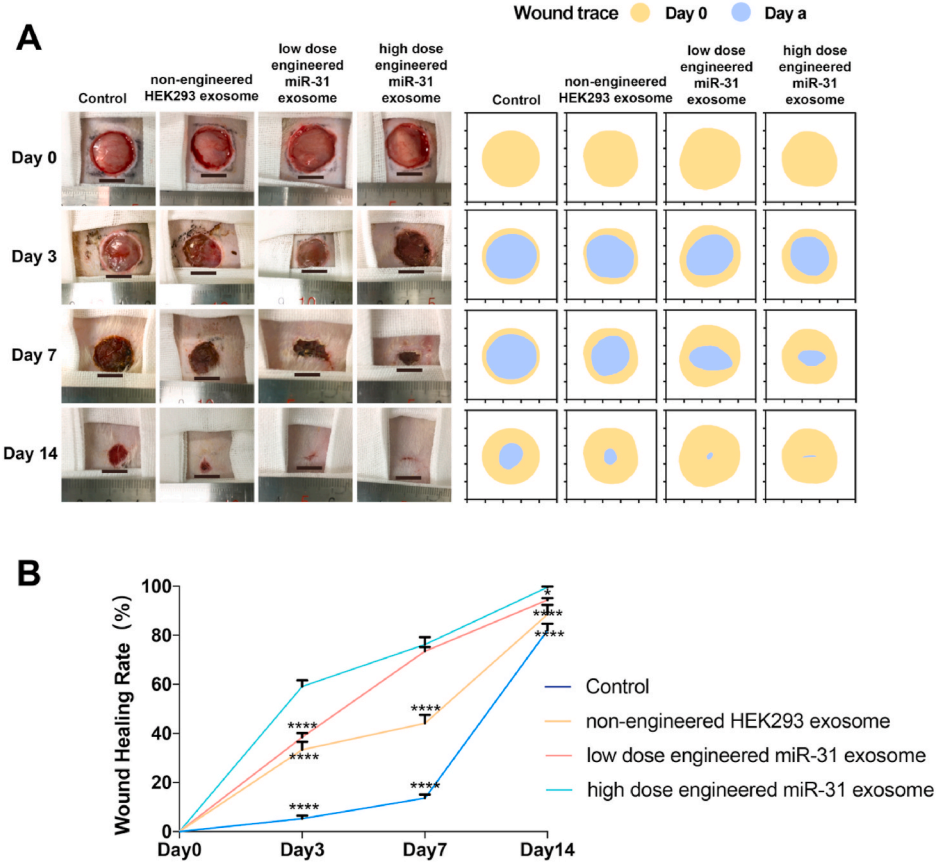

Fig. 5. Diabetic wound closure after treatment with engineered miR-31 exosomes. (A) General observation of diabetic wounds under different conditions; (B) healing rate of diabetic wounds under different conditions; *significant difference compared with high-dose engineered miR-31 exosomes ($p < 0.05$); **significant difference compared with high-dose engineered miR-31 exosomes ($p < 0.01$); ***significant difference compared with high-dose engineered miR-31 exosomes ($p < 0.001$); ****significant difference compared with high-dose engineered miR-31 exosomes ($p < 0.0001$).

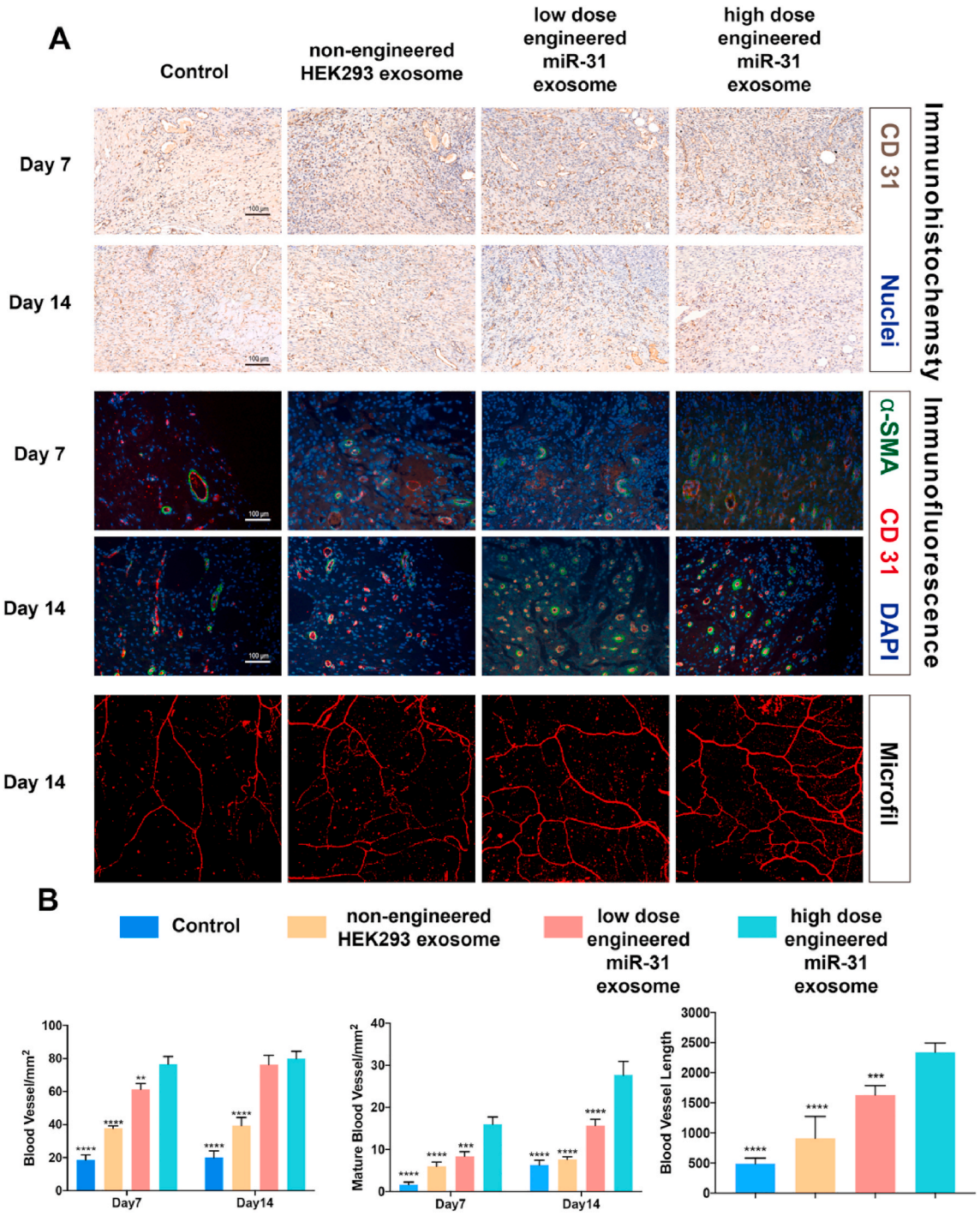

Fig. 6. Angiogenesis in diabetic wounds. (A) Representative image of immunohistochemistry (CD31), immunofluorescence (CD31/α-SMA) and a 3D-reconstructed image of newly formed capillaries; (B) quantitative angiogenesis data; *significant difference compared with high-dose engineered miR-31 exosomes ($p < 0.05$); **significant difference compared with high-dose engineered miR-31 exosomes ($p < 0.01$); ***significant difference compared with high-dose engineered miR-31 exosomes ($p < 0.001$); ****significant difference compared with high-dose engineered miR-31 exosomes ($p < 0.0001$).

transfection. The engineered miR-31-5p exosomes were obtained by collecting exosomes secreted by stably transfected cell lines. Multiple technologies were then used to characterize the engineered miR-31-5p exosomes. According to TEM and DLS, spherical microvesicles ranged from 30 to 150 nm, which indicated our successful isolation of the nonengineered HEK293 exosomes and the engineered miR-31 exosomes (Fig. 3A). Western blotting for surface markers further confirmed their successful isolation (Fig. 3B). However, these two types of exosomes could not be distinguished based on morphology and surface markers. Not all miRNAs can be enriched and encapsulated by exosomes. Therefore, we used qRT-PCR to detect miR-31 expression in the engineered miR-31 exosomes. The results showed that the engineered miR-31 exosomes expressed substantially higher miR-31-5p levels than the nonengineered HEK 293 exosomes, which indicates that miR-31-5p can be enriched in engineered exosomes (Fig. 3E). Exosomes should be phagocytized into cells to exert their effects (Fig. 3C). Uptake of the two types of exosomes by the three cell lines was observed via laser confocal microscopy, which showed that both exosome types could be well-

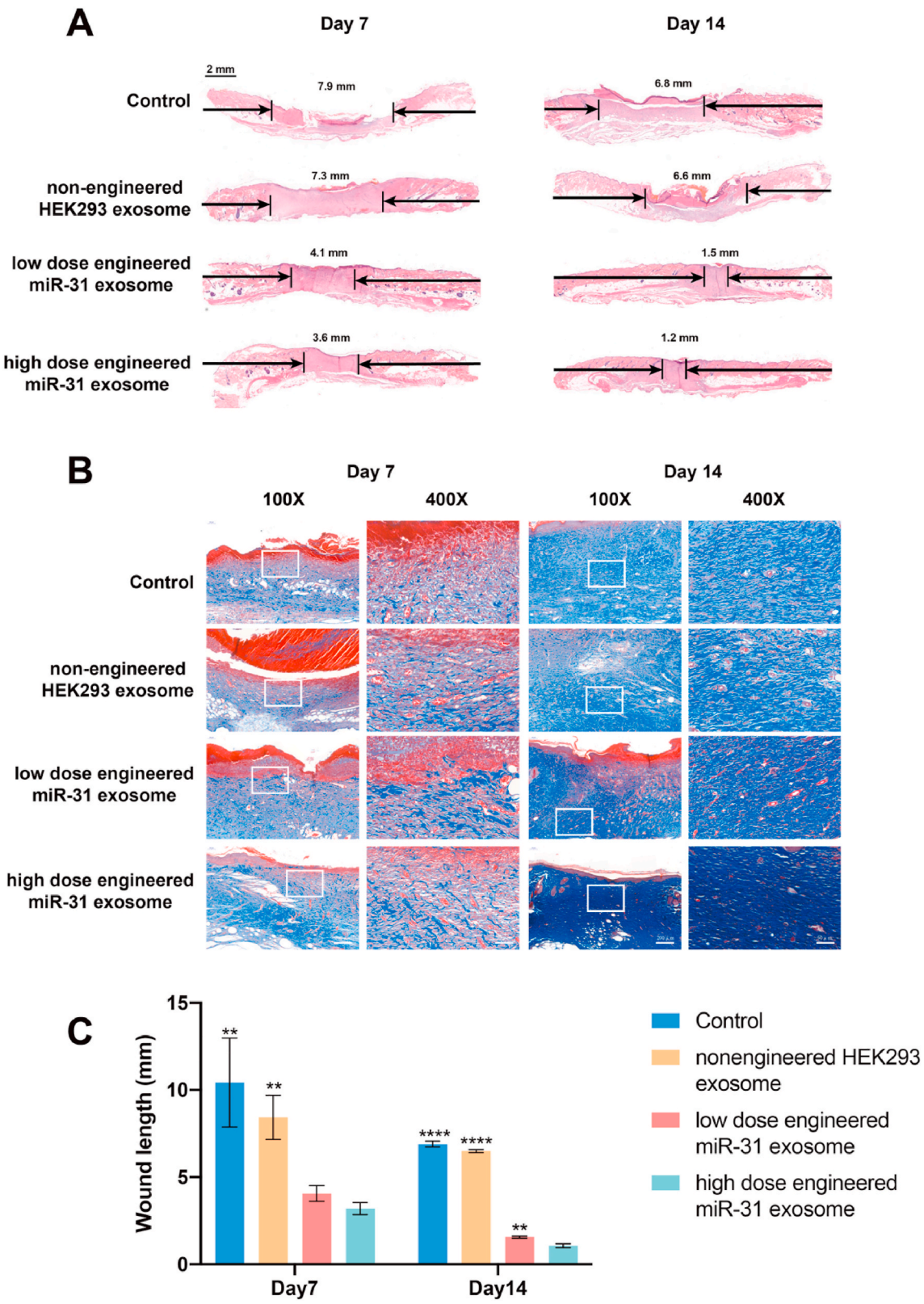

Fig. 7. Collagen deposition and reepithelization in diabetic wounds. (A) H&E staining of a healing wound; (B) Masson's trichrome revealed collagen deposition in wounds; (C) quantitative wound healing data; *significant difference compared with high-dose engineered miR-31 exosomes ($p < 0.05$); **significant difference compared with high-dose engineered miR-31 exosomes ($p < 0.01$); ***significant difference compared with high-dose engineered miR-31 exosomes ($p < 0.001$); ****significant difference compared with high-dose engineered miR-31 exosomes ($p < 0.0001$).

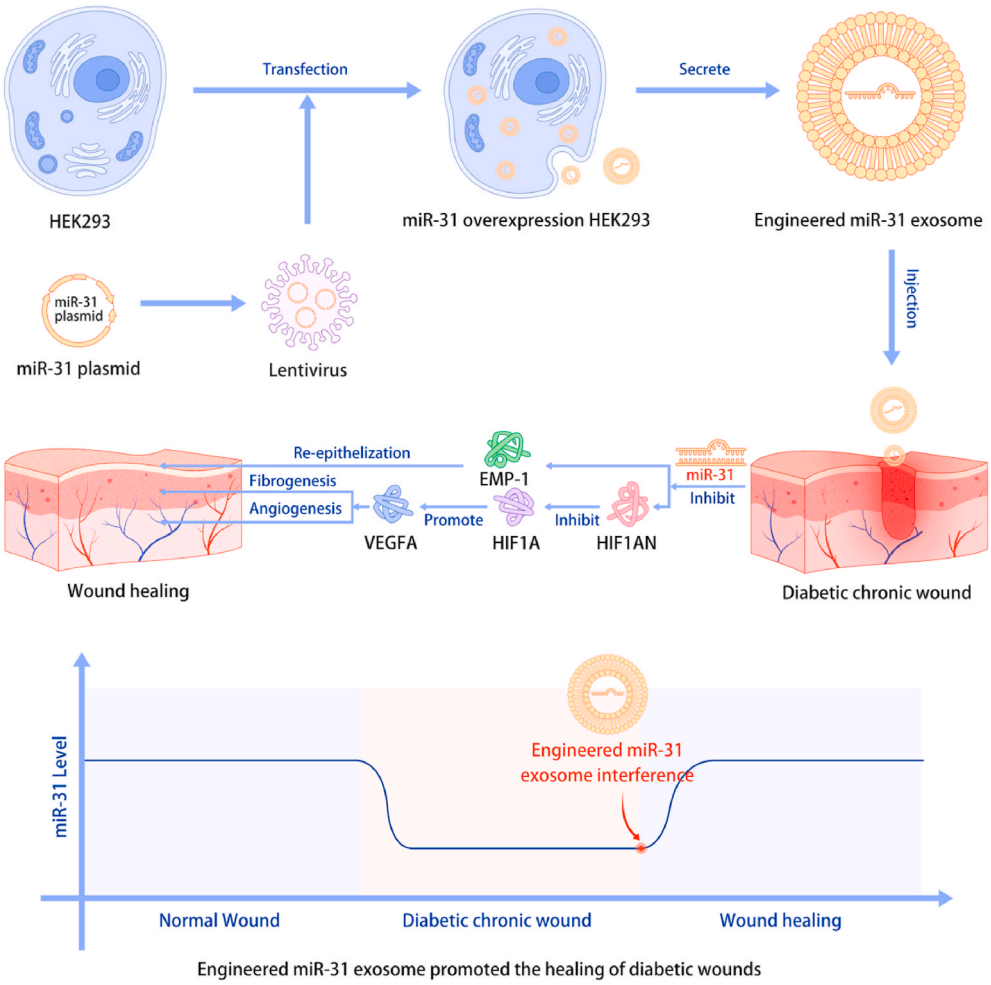

Fig. 8. Research scheme of engineered miR-31 exosome development and the mechanism of action in diabetic wound healing.

phagocytized by the three wound-related cell lines. qRT-PCR for miR-31-5p (Fig. 3D) showed that miR-31-5p expression in the three wound healing-related cell types was promoted by the engineered miR-31 exosomes.

To determine the efficacy of the engineered miR-31 exosomes in diabetic wound healing, we first performed in vitro experiments. The engineered miR-31 exosomes promoted cell proliferation (Fig. 4B) and migration (Fig. 4A) in ECs, HFF-1 cells and HaCaT cells. The engineered miR-31 exosomes also promoted capillary-like construction activity of ECs (Fig. 4C). Our data indicated that the engineered miR-31 exosomes can positively regulate the three cell types and therefore have the potential to close chronic diabetic wounds. Furthermore, we performed in vivo experiments to evaluate the effects of the engineered miR-31 exosomes in diabetic wound healing.

3.4. *Engineered miR-31 exosomes promote the healing of diabetic wounds in rats via proangiogenesis, profibrogenesis and reepithelization effects*

In vivo, the wound-healing process and rate were observed. Angiogenesis, fibrogenesis and reepithelization are three key processes in wound healing that were observed in the in vivo study.

No significant adverse conditions or complications were observed throughout the duration of the experiment. Wound closure progressed from 0 to 14 days and was recorded and quantified using digital images (Fig. 5A and B). The results showed that the wounds of the engineered miR-31 exosome-treated group were smaller than those of the non-engineered HEK293 exosome-treated group and were substantially smaller than those of the control group on days 3 and 7. On day 14, the wounds of the engineered miR-31 exosome-treated group were almost closed, while those of the control group and the nonengineered HEK293 exosome group remained unclosed.

Angiogenesis was assessed via micro-CT, immunofluorescence and immunohistochemistry (Fig. 6, Fig. S2). Micro-CT 3-dimensional reconstructed images revealed substantially denser blood vessels in the wounds of the engineered miR-31 exosome group than the non-engineered exosome group, which had denser blood vessels than the control group. Quantification of the newly formed vessel area and number further confirmed the 3-dimensional reconstructed images. Immunohistochemical staining for CD31 and immunofluorescence staining for CD31 and α-SMA revealed the numbers of newly formed and mature blood vessels in wounds of the different groups. Qualitative and quantified data showed denser blood vessels and more mature vessels in the engineered miR-31 exosome-treated wounds than in the wounds of the other groups at both 7 and 14 days. These results suggest that the engineered miR-31 exosomes promote angiogenesis in chronic diabetic wounds and that the effects are stronger than those of the nonengineered HEK293 exosomes.

H&E staining showed reepithelization 7 and 14 days after surgery (Fig. 7A and C). The results showed that neoepithelium lengths and wound closure were significantly better in the engineered miR-31 exosome group than in the nonengineered HEK293 exosome and control groups. The wounds treated with the engineered miR-31 exosomes were almost closed, and the neoepithelium covered the entire wound, while in the control group, the wounds were only 50% covered. Moreover, more

constructs resembling hair follicles and sebaceous glands were evident in the engineered miR-31 exosome group and the nonengineered exosome group than in the control group.

Masson's trichrome staining (Fig. 7B) revealed differences in collagen deposition and composition between different groups during wound healing. Compared with the control group wounds, the wounds treated with the nonengineered exosomes had larger amounts of collagen deposition and thicker wavy collagen fibers. However, the wounds treated with the engineered miR-31 exosomes showed more collagen deposition than those treated with the nonengineered exosomes, and the arrangement of wavy collagen fibers was similar to that in normal skin.

The in vivo study revealed that engineered miR-31 exosomes promoted the healing rate of diabetic wounds via proangiogenesis, profibrogenesis and reepithelization and their synergistic effects. The engineered miR-31 exosomes, therefore, are a multifunctional and highly efficient nanomaterial for diabetic wound healing. However, this study still has some limitations. We used a cell line as an exosome-producing factory, which limits the clinical translation of this study. Although many scholars believe that exosomes are not tumorigenic, no long-term clinical observational data regarding this issue have been published. We have attempted to use stem cells as exosome factories; however, the stable transformation efficiency of stem cells is too low to be useful. In future research, we will explore better ways to produce exosomes.

4. Conclusion

The present study described the development of a novel RNAi therapy: disease-initiated miRNAi therapy. We identified a crucial miRNA, miR-31-5p, in diabetic wound pathophysiology. MiR-31-5p is a multifunctional factor in the angiogenesis, fibrogenesis and reepithelization processes, and the exact mechanisms related to the HIF pathway and EMP-1 were determined. Exosomes were then applied as nanocarriers of miR-31-5p. Using engineered miR-31 exosomes, diabetic wounds were rapidly closed via proangiogenesis, profibrogenesis and reepithelization. Together, these results indicate that engineered miR-31 exosomes are a disease pathophysiology-initiated nanomaterial and a precision therapy for diabetic chronic wound treatment (Fig. 8).

CRediT authorship contribution statement

Jinghuan Huang: Conceptualization, Methodology, Investigation, Data curation, Writing - original draft, Writing - review & editing. **Muyu Yu:** Methodology, Investigation, Data curation. **Wenjing Yin:** Funding acquisition, Investigation. **Bo Liang:** Methodology. **Ang Li:** Methodology, Investigation. **Jingfeng Li:** Funding acquisition, Investigation. **Xiaolin Li:** Project administration, Supervision, Funding acquisition, Conceptualization, Data curation, Writing - review & editing. **Shichang Zhao:** Project administration, Funding acquisition. **Fang Liu:** Project administration, Supervision, Funding acquisition.

Declaration of competing interest

None.

Acknowledgments

The authors acknowledge the support of the National Natural Science Foundation of China (81572178, 81270397, 81702317, 81871752 and 81770802), the National Key R & D Program of China (2017YFC1309601 to Fang Liu), Shanghai Municipal Commission of Health and Family Planning under the fund (20124356) and a Shanghai Municipal Education Commission-Gaofeng Clinical Medicine Grant (20152232).

Appendix A. Supplementary data

Supplementary data to this article can be found online at https://doi.org/10.1016/j.bioactmat.2021.02.007.

References

[1] Y. Shin Ko, H. Jin, S. Won Park, H. Jung Kim, Salvianolic acid B protects against oxLDL-induced endothelial dysfunction under high-glucose conditions by downregulating ROCK1-mediated mitophagy and apoptosis, Biochem. Pharmacol. (2020) 113815.
[2] S. Hamed, Y. Ullmann, D. Egozi, E. Daod, E. Hellou, M. Ashkar, A. Gilhar, L. Teot, Fibronectin potentiates topical erythropoietin-induced wound repair in diabetic mice, J. Invest. Dermatol. 131 (6) (2011) 1365–1374.
[3] H. Thangarajah, D. Yao, E.I. Chang, Y. Shi, L. Jazayeri, I.N. Vial, R.D. Galiano, X. L. Du, R. Grogan, M.G. Galvez, M. Januszyk, M. Brownlee, G.C. Gurtner, The molecular basis for impaired hypoxia-induced VEGF expression in diabetic tissues, Proc. Natl. Acad. Sci. U. S. A. 106 (32) (2009) 13505–13510.
[4] M. Deveci, R.R. Gilmont, W.R. Dunham, B.P. Mudge, D.J. Smith, C.L. Marcelo, Glutathione enhances fibroblast collagen contraction and protects keratinocytes from apoptosis in hyperglycaemic culture, Br. J. Dermatol. 152 (2) (2005) 217–224.
[5] S. Tyeb, P.A. Shiekh, V. Verma, A. Kumar, Adipose-Derived stem cells (ADSCs) loaded gelatin-sericin-laminin cryogels for tissue regeneration in diabetic wounds, Biomacromolecules 21 (2) (2020) 294–304.
[6] Y.X. Lin, Y. Wang, S. Blake, M. Yu, L. Mei, H. Wang, J. Shi, RNA nanotechnology-mediated cancer immunotherapy, Theranostics 10 (1) (2020) 281–299.
[7] S. Bajan, G. Hutvagner, RNA-based therapeutics: from antisense oligonucleotides to miRNAs, Cells 9 (1) (2020).
[8] K. Takakura, A. Kawamura, Y. Torisu, S. Koido, N. Yahagi, M. Saruta, The clinical potential of oligonucleotide therapeutics against pancreatic cancer, Int. J. Mol. Sci. 20 (13) (2019).
[9] R. Alzhrani, H.O. Alsaab, A. Petrovici, K. Bhise, K. Vanamala, S. Sau, M.J. Krinock, A.K. Iyer, Improving the therapeutic efficiency of noncoding RNAs in cancers using targeted drug delivery systems, Drug Discov. Today 25 (4) (2019) 718–730.
[10] G. Mahmoodi Chalbatani, H. Dana, E. Gharagouzloo, S. Grijalvo, R. Eritja, C. D. Logsdon, F. Memari, S.R. Miri, M.R. Rad, V. Marmari, Small interfering RNAs (siRNAs) in cancer therapy: a nano-based approach, Int. J. Nanomed. 14 (2019) 3111–3128.
[11] S.W. Young, M. Stenzel, J.L. Yang, Nanoparticle-siRNA: a potential cancer therapy? Crit. Rev. Oncol. Hematol. 98 (2016) 159–169.
[12] S. Colombo, X. Zeng, H. Ragelle, C. Foged, Complexity in the therapeutic delivery of RNAi medicines: an analytical challenge, Expet Opin. Drug Deliv. 11 (9) (2014) 1481–1495.
[13] Y. Weng, Q. Huang, C. Li, Y. Yang, X. Wang, J. Yu, Y. Huang, X.J. Liang, Improved nucleic acid therapy with advanced nanoscale biotechnology, Mol. Ther. Nucleic Acids 19 (2019) 581–601.
[14] X. Li, C. Li, L. Zhang, M. Wu, K. Cao, F. Jiang, D. Chen, N. Li, W. Li, The significance of exosomes in the development and treatment of hepatocellular carcinoma, Mol. Canc. 19 (1) (2020) 1.
[15] H.S. Joo, J.H. Suh, H.J. Lee, E.S. Bang, J.M. Lee, Current knowledge and future perspectives on mesenchymal stem cell-derived exosomes as a new therapeutic agent, Int. J. Mol. Sci. 21 (3) (2020).
[16] X. Zhou, Z. Li, W. Sun, G. Yang, C. Xing, L. Yuan, Delivery efficacy differences of intravenous and intraperitoneal injection of exosomes:perspectives from tracking dye labeled and MiRNA encapsulated exosomes, Curr. Drug Deliv. 17 (3) (2020) 186–194.
[17] T. Yong, X. Zhang, N. Bie, H. Zhang, X. Zhang, F. Li, A. Hakeem, J. Hu, L. Gan, H. A. Santos, X. Yang, Tumor exosome-based nanoparticles are efficient drug carriers for chemotherapy, Nat. Commun. 10 (1) (2019) 3838.
[18] A. Familtseva, N. Jeremic, S.C. Tyagi, Exosomes: cell-created drug delivery systems, Mol. Cell. Biochem. 459 (1–2) (2019) 1–6.
[19] S.C. Tao, Y.S. Gao, H.Y. Zhu, J.H. Yin, Y.X. Chen, Y.L. Zhang, S.C. Guo, C.Q. Zhang, Decreased extracellular pH inhibits osteogenesis through proton-sensing GPR4-mediated suppression of yes-associated protein, Sci. Rep. 6 (2016) 26835.
[21] T. Umezu, H. Tadokoro, K. Azuma, S. Yoshizawa, K. Ohyashiki, J.H. Ohyashiki, Exosomal miR-135b shed from hypoxic multiple myeloma cells enhances angiogenesis by targeting factor-inhibiting HIF-1, Blood 124 (25) (2014) 3748–3757.
[22] J.R. Guo, L. Yin, Y.Q. Chen, X.J. Jin, X. Zhou, N.N. Zhu, X.Q. Liu, H.W. Wei, L. S. Duan, Autologous blood transfusion augments impaired wound healing in diabetic mice by enhancing lncRNA H19 expression via the HIF-1alpha signaling pathway, Cell Commun. Signal. 16 (1) (2018) 84.
[23] D.F. Higgins, K. Kimura, W.M. Bernhardt, N. Shrimanker, Y. Akai, B. Hohenstein, Y. Saito, R.S. Johnson, M. Kretzler, C.D. Cohen, K.U. Eckardt, M. Iwano, V. H. Haase, Hypoxia promotes fibrogenesis in vivo via HIF-1 stimulation of epithelial-to-mesenchymal transition, J. Clin. Invest. 117 (12) (2007) 3810–3820.
[24] D. Li, X.I. Li, A. Wang, F. Meisgen, A. Pivarcsi, E. Sonkoly, M. Stahle, N.X. Landen, MicroRNA-31 promotes skin wound healing by enhancing keratinocyte proliferation and migration, J. Invest. Dermatol. 135 (6) (2015) 1676–1685.
[25] Y. Gao, Z. Xie, C. Ho, J. Wang, Q. Li, Y. Zhang, J. Zhou, LRG1 promotes keratinocyte migration and wound repair through regulation of HIF-1alpha stability, J. Invest. Dermatol. 140 (2) (2020) 455–464 e8.

[26] L. Zhou, Y. Wang, M. Zhou, Y. Zhang, P. Wang, X. Li, J. Yang, H. Wang, Z. Ding, HOXA9 inhibits HIF-1alpha-mediated glycolysis through interacting with CRIP2 to repress cutaneous squamous cell carcinoma development, Nat. Commun. 9 (1) (2018) 1480.
[27] J. Bruck, R. Dringen, A. Amasuno, I. Pau-Charles, K. Ghoreschi, A review of the mechanisms of action of dimethylfumarate in the treatment of psoriasis, Exp. Dermatol. 27 (6) (2018) 611–624.
[28] R.R. Wong, N. Abd-Aziz, S. Affendi, C.L. Poh, Role of microRNAs in antiviral responses to dengue infection, J. Biomed. Sci. 27 (1) (2020) 4.
[29] R. Titze-de-Almeida, C. David, S.S. Titze-de-Almeida, The race of 10 synthetic RNAi-based drugs to the pharmaceutical market, Pharm. Res. (N. Y.) 34 (7) (2017) 1339–1363.
[30] J. Moura, A. Sorensen, E.C. Leal, R. Svendsen, L. Carvalho, R.J. Willemoes, P. T. Jorgensen, H. Jenssen, J. Wengel, L.T. Dalgaard, E. Carvalho, microRNA-155 inhibition restores Fibroblast Growth Factor 7 expression in diabetic skin and decreases wound inflammation, Sci. Rep. 9 (1) (2019) 5836.
[31] B. Kim, J.H. Park, M.J. Sailor, Rekindling RNAi therapy: materials design requirements for in vivo siRNA delivery, Adv. Mater. 31 (49) (2019), e1903637.
[32] J. Majumder, O. Taratula, T. Minko, Nanocarrier-based systems for targeted and site specific therapeutic delivery, Adv. Drug Deliv. Rev. 144 (2019) 57–77.
[33] P.A. Shiekh, A. Singh, A. Kumar, Exosome laden oxygen releasing antioxidant and antibacterial cryogel wound dressing OxOBand alleviate diabetic and infectious wound healing, Biomaterials 249 (2020) 120020.
[34] Y. Xiong, L. Chen, C. Yan, W. Zhou, Y. Endo, J. Liu, L. Hu, Y. Hu, B. Mi, G. Liu, Circulating exosomal miR-20b-5p inhibition restores Wnt9b signaling and reverses diabetes-associated impaired wound healing, Small 16 (3) (2020), e1904044.
[35] H. Kim, S.Y. Wang, G. Kwak, Y. Yang, I.C. Kwon, S.H. Kim, Exosome-guided phenotypic switch of M1 to M2 macrophages for cutaneous wound healing, Adv. Sci. 6 (20) (2019) 1900513.
[36] M. Wang, C. Wang, M. Chen, Y. Xi, W. Cheng, C. Mao, T. Xu, X. Zhang, C. Lin, W. Gao, Y. Guo, B. Lei, Efficient angiogenesis-based diabetic wound healing/skin reconstruction through bioactive antibacterial adhesive ultraviolet shielding nanodressing with exosome release, ACS Nano 13 (9) (2019) 10279–10293.
[37] P.A. Shiekh, A. Singh, A. Kumar, Data supporting exosome laden oxygen releasing antioxidant and antibacterial cryogel wound dressing OxOBand alleviate diabetic and infectious wound healing, Data Brief 31 (2020) 105671.
[38] J. Phan, P. Kumar, D. Hao, K. Gao, D. Farmer, A. Wang, Engineering mesenchymal stem cells to improve their exosome efficacy and yield for cell-free therapy, J. Extracell. Vesicles 7 (1) (2018) 1522236.
[39] J.P.K. Armstrong, M.M. Stevens, Strategic design of extracellular vesicle drug delivery systems, Adv. Drug Deliv. Rev. 130 (2018) 12–16.
[40] I.L. Colao, R. Corteling, D. Bracewell, I. Wall, Manufacturing exosomes: a promising therapeutic platform, Trends Mol. Med. 24 (3) (2018) 242–256.